Swimming in Potential Flow

Thesis by
Alec Glisman

In Partial Fulfillment of the Requirements for the
Degree of
Master of Science in Chemical Engineering

CALIFORNIA INSTITUTE OF TECHNOLOGY
Pasadena, California

2022
Submitted December 6, 2021

Alec Glisman
ORCID: 0000–0001–9677–1958

ACKNOWLEDGEMENTS

I want to thank Professor John Brady for his patience, guidance, and mentorship throughout the last few years. His ability to distill complex models into key physical ideas and relate them to others has amazed me in research and the classroom.

The members of the Brady group have been instrumental to my success at Caltech. I am indebted to them all for answering a myriad of questions and welcoming me into the group with such kindness. Camilla Kjeldbjerg not only had great scientific ideas but always had something fun to discuss. Hyeongjoo Row and Zhiwei Peng were superb teaching assistants in my core graduate courses and contributed significantly to my academic success. Benjamin Ye was a great collaborator in our shared courses. Dr. Stewart Mallory and Dr. Edmond Zhou were wonderful mentors for advancing my skills in scientific computing and developing independent code-bases. Most notably, I would like to thank Austin Dulaney. His support and concern kept me motivated, especially as I felt overwhelmed balancing research and coursework in my first year as a graduate student.

Finally, I wish to thank my family. My mother and father have sacrificed immensely throughout their lives to allow me to pursue my dreams. My sister, Hannah, has kept me grounded. Kayla has been a constant source of positivity and strength through adversity. Ravi continually challenges my views of both science and the world.

I am grateful for those listed above and so many others throughout my life.

ABSTRACT

Active bodies undergo self-propulsive motion in a fluid medium and span a broad range of length and time scales. This report focuses specifically on the motion at high Reynolds number, where inertial forces dominate the fluid dynamics. Many active systems spontaneously self-organize into visually striking structures: fish schooling, birds flocking, and bacterial colonies growing. Current models of emergent behavior in the inertial regime are mainly phenomenological and do not account for the fluid-mediated interactions between bodies. We seek to advance physical models of swimmers in high inertia environments. To this end, we explicitly model the hydrodynamics to discern what role the fluid medium plays in active group dynamics and whether it can reproduce the observed emergent phenomenon without the imposition of phenomenologically based interaction rules.

A minimal swimmer model consisting of three linked spheres is constructed, and we find self-propulsion without external forces or momentum transfer via vortex shedding. The inertial swimmer is also compared to an identical swimmer in the Stokes regime—where fluid inertia is neglected. The Stokes hydrodynamics are longer-ranged at leading order, and we demonstrate that the stronger hydrodynamic interactions lead to a greater center of mass translation after a period of articulation.

TABLE OF CONTENTS

LIST OF ILLUSTRATIONS

LIST OF SYMBOLS

a	radius of spherical particle
α, β, γ	indices representing particle number
$\nabla(\cdot)$	Cartesian gradient
$\nabla^2(\cdot)$	Cartesian Laplacian
$\partial\Omega_\alpha$	surface of particle α
δ	angular phase shift
δ_{ij}	Kronecker delta
E	energy
$\mathbf{e}$	symmetric rate of strain tensor
$\boldsymbol{e}_i$	Cartesian coordinate basis vectors
$\mathbf{F}$	force
Γ	ratio of particle to fluid mass density
$\mathscr{H}$	Hamiltonian
$\mathbf{I}$	identity tensor
i, j, k	indices representing each individual entry in a tensor/vector
$\mathbf{L}$	torque
L	characteristic length scale
$\mathscr{L}$	Lagrangian
$\boldsymbol{M}_{\alpha\beta}$	added mass between particles α and β
$\hat{\mathbf{M}}$	Stokes mobility tensor
$\mathscr{M}_{\alpha\beta}$	total mass between particles α and β
μ	fluid viscosity
N	number of particles
$\boldsymbol{n}$	normal vector to particle surface, pointing outwards by convention
ν	fluid mass displaced by a single particle

$\boldsymbol{\Omega}$	angular velocity
ω	frequency
$\otimes$	dyadic product
$\mathbf{P}_\alpha$	linear momentum of particle α
$\mathrm{P}^{(t)}$	total linear momentum
$\boldsymbol{\Phi}$	generalized solution to Laplace's equation
ϕ	scalar velocity potential
p	fluid pressure
$\boldsymbol{r}$	radial distance vector
$\boldsymbol{R}_\alpha$	center of solid particle α
$\hat{\mathbf{R}}$	Stokes resistance tensor
$\boldsymbol{\mathcal{R}}$	Rayleigh dissipation tensor
ρ	mass density
$\mathbf{S}$	Stokes stresslet
t	time
$\mathscr{T}$	kinetic energy
$\dot{(\cdot)}$	time rate of change
$\boldsymbol{U}_\alpha$	velocity of particle α
$\dot{\boldsymbol{U}}_\alpha$	acceleration of particle α
u^2	velocity field L-2 vector norm squared
V	volume
$\mathscr{V}$	potential energy
$\boldsymbol{x}$	position in Cartesian space
X, Y, Z	generalized internal spatial coordinates for a body

Chapter 1

HYDRODYNAMICS/INTRODUCTION

Active matter is a class of materials that generate their own propulsive force. Net motion typically results from phoresis [1] or internal body deformations [2–4]. In Fig. 1.1, we depict several common examples of active matter systems across a broad range of length scales. Both fish and birds deform their bodies to generate a propulsive force within their respective fluid media [5]. At the microscopic scale, bacteria such as *E. coli* rotate a flagellar bundle to shear the fluid and propel forwards [6]. Active systems can also be synthesized in a variety of forms, with Janus spheres being one of the most commonly studied [10]. Janus spheres catalyze a chemical decomposition on one hemisphere and self-propel via diffusiophoresis—effectively becoming nano-motors with

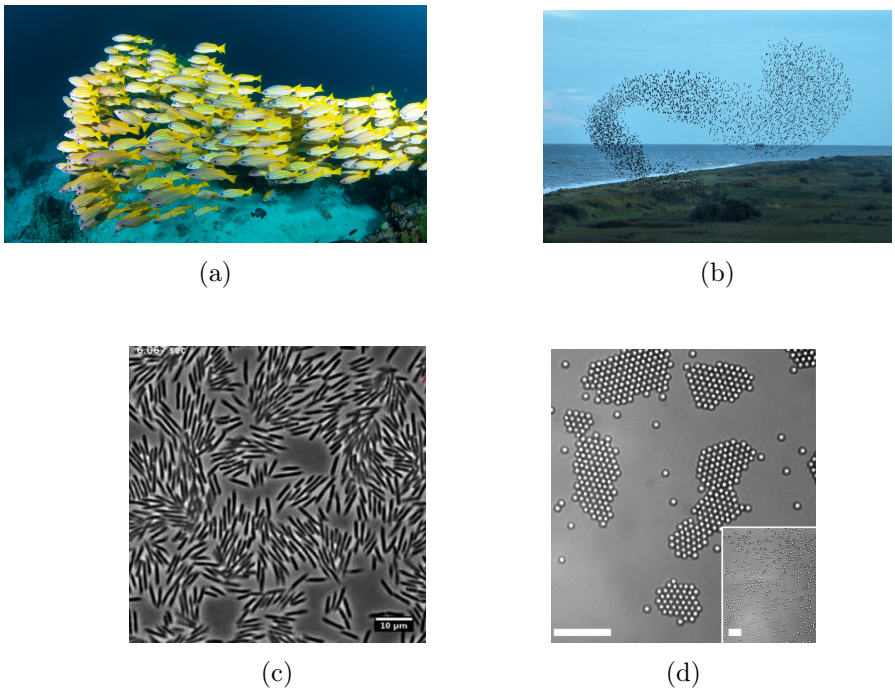

(a) (b)

(c) (d)

Figure 1.1: Macroscopic examples [7] of emergent phenomena: () fish schooling and (a) starlings flocking. Self-propulsive bodies also aggregate in the microscopic regime. (b) *E. coli* swarm [8] and align with nearest neighbors. (c) Light-activated Janus particles [9] cluster from a homogenous distribution (inset) as light catalyzes phoretic motion (scale bar 10 μm).

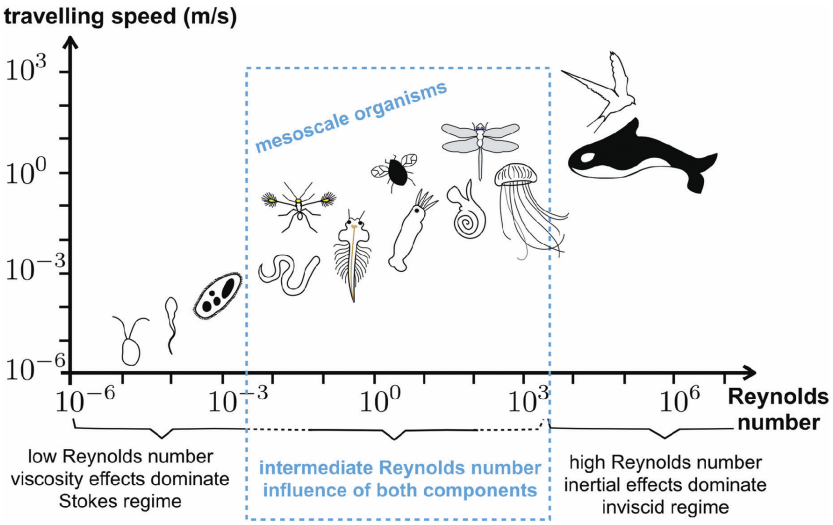

Figure 1.2: Reynolds numbers of swimming and flying animals from Ref. [23]. Organisms from left to right: algae, bacterium, paramecium, nematode, fairyfly, brine shrimp, larval squid, wasp, pteropod, dragonfly, jellyfish, whale, swallow.

no moving parts [11, 12]. We are especially interested in the fluid mediated interactions between self-propulsive bodies and how they may lead to collective behavior. An individual body, such as a fish or bird, creates a fluid disturbance and impacts the fluid forces on all other bodies in the system.

The essential fluid mechanics vary between the microscopic and macroscopic regimes and are characterized by the Reynolds number, $\mathrm{Re} := \rho\,\mathrm{U}\,\mathrm{L}\,/\mu$, which spans many orders of magnitude in swimming and flying organisms (Fig. 1.2). The Reynolds number quantifies the relative importance of inertial to viscous forces in the fluid medium, [13–15] where the density ρ and viscosity μ of the fluid are material parameters. The characteristic length L and velocity U scales in our systems are set by a body's length and average swim speed. For microscopic systems, both characteristic velocity and length scales tend to be "small" such that $\mathrm{Re} \ll 1$, and the fluid equations of motion reduce to the linear Stokes equations.

Self-propulsion in the Stokes regime has been extensively studied. There is considerable knowledge about individual swimming mechanisms [2, 4, 16–19] and the interactions between swimming bodies that give rise to emergent phenomena [20–22]. However, larger bodies, such as birds and fish, self-propel at high Reynolds numbers. With common material parameters [24, 25] and assumed characteristic scales of $\mathrm{L} = 0.1\,\mathrm{m}$ and $\mathrm{U} = 0.1\,\mathrm{m/s}$ as a rough esti-

mate for both birds and fish, the Reynolds number for self-propulsion in air and water is 6×10^2 and 1×10^4, respectively. The fluid inertia cannot be neglected at moderate and large Reynolds numbers, posing a major issue. The inertial forces are non-linear and make solving the Navier-Stokes equations much more computationally expensive. Of course, a finite element scheme for the fluid with deformable solid bodies can be constructed. This method works very well with a few swimmers, especially when paired with statistical learning techniques [26]. However, collective phenomena by definition require large numbers of bodies, $O(10^3)$, and the full fluid mechanical solution becomes computationally intractable at this limit.

Historically, modeling emergent phenomena at high Reynolds number has sidestepped the Navier-Stokes equations by neglecting the fluid medium entirely. The models instead introduce phenomenological rules for body interactions that lead to collective behavior. One of the most widespread frameworks, the Vicsek model [27], assumes that each body will align its velocity vector with the average of its nearest neighbors—with added noise to prevent all trajectories from collapsing. The Vicsek model has also been generalized to account for more complex interactions between group members by incorporating relative orientational and rotational interactions [28–31]. While the Vicsek model can reproduce the group dynamics seen in fish schooling and birds flocking, the model only provides a phenomenological basis for the observed phenomena. We would like to understand if the imposed "intelligence" is necessary for collective effects or if we can reproduce the same phenomena using a simple, mechanical model that explicitly accounts for fluid interactions.

If we additionally approximate the fluid flow as irrotational, we can apply potential flow theory to create a much simpler model of the many-body hydrodynamic interactions [32–36]. The irrotational restriction is admittedly severe, and we are neglecting a physical phenomenon that has often been considered essential [5, 37, 38] for self-propulsion in high Reynolds flow: vortex shedding through the momentum boundary layer. Vorticity naturally exists in the wake and boundary layer surrounding the bodies, which may account for some aspect of collective motion. However, the vorticity sources have been shown to scale inversely with the Reynolds number for spherical bodies [39] and

so might not be critical for certain classes of swimmers. Before discussing the feasibility of self-propulsion in potential flow, we begin with a few comments on how a potential flow may lead to collective effects.

In potential flow at high Reynolds number, the steady flow fields reduce to the well-known Bernoulli's equation

$$p + \frac{1}{2}\rho u^2 = \text{constant} \ , \tag{1.1}$$

which states that the fluid velocity and pressure are in a constant balance. Two particles that are translating parallel to each other (Fig. 1.3a) cause the fluid between their line of centers to flow faster relative to the background velocity. By Bernoulli's equation, there exists a pressure minima at their central point and the fluid effectively attracts the two particles along their common axis. Potential flow then presents a physical mechanism for bodies

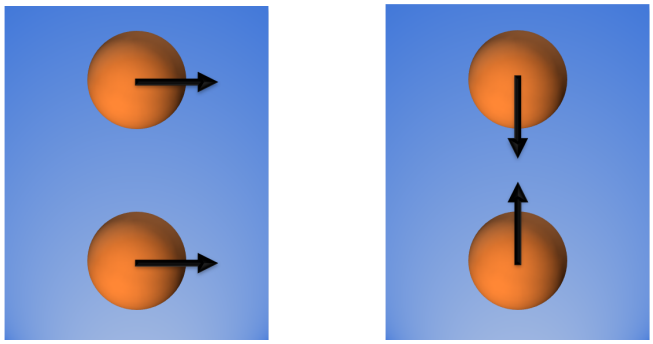

(a) (b)

Figure 1.3: (a) Two particles translating parallel to one another are attracted and (b) are repelled when translating towards their mutual center.

to aggregate and may be a source of emergent phenomena. If two particles are instead translating towards one another (Fig. 1.3b), they must push the fluid out from their line of center. By symmetry, a stagnation point exists at the pair's central point, leading to a pressure maxima and fluid repulsive forces. As the fluid can both attract and repel bodies [40], it may therefore set a natural interaction length scale and aid in modeling collective phenomena.

Bubbly liquids, which possess the same fluid mechanics as the high Reynolds swimmers, have been shown to spontaneously cluster when rising due to buoyant forces [35]. As viscous dissipation is neglected at high Reynolds number, the system is also conservative and therefore has a constant Lagrangian and

Hamiltonian. The hydrodynamic interactions were derived through the Lagrangian, which is found to possess a configuration-dependent added mass. The added mass physically captures the effective increase in inertia that a particle experiences from the fluid when translating in potential flow. Through Hamiltonian mechanics, the added mass can be viewed as an effective potential and lead to the thermodynamic order-disorder phase transition. We want to study whether this aggregation also occurs in high Reynolds number active systems.

Now that the possible mechanism for collective phenomena seen in Fig. 1.1 has been shown for potential flow, we return to the issue of self-propulsion. We have made two crucial fluid mechanical assumptions: the fluid flow is inviscid and irrotational. As we will show, viscous drag forces can be added by using the Rayleigh dissipation function in the Lagrangian framework [41, 42]. However, the irrotational approximation cannot be relaxed in potential flow, and we must ask if vorticity is an essential element for self-propulsion. Is a single fish or bird able to self-propel in an inviscid potential flow without modeling boundary layers? Thankfully, the answer is a resounding yes, and vorticity is not needed for self-propulsion at high Reynolds number. Saffman first demonstrated that net motion is possible for an inviscid swimmer in potential flow [3]. The result is especially interesting, as the net motion occurs without energetic dissipation. Saffman argued that by breaking the natural time-reversal symmetry inherent in an inviscid and irrotational flow, propulsion could be generated from the configuration-dependent hydrodynamic forces. Kanso & Marsden have continued to study self-propulsion in inviscid, irrotational flows by modeling a swimmer as a collection of two-dimensional ellipsoids that are connected via hinges [36, 43, 44]. Using control theory, they determined the optimal articulation for their swimmer design.

The question of what body deformations result in self-propulsion has been long debated in Stokes regime flows. Interestingly, both potential flow and Stokes flow have time-reversible fluid dynamics. Purcell first hypothesized (without mathematical proof) the general deformation requirements for a Stokes swimmer in what is now referred to as the Scallop Theorem [45]. The Scallop Theorem states that in the time-reversible Stokes medium, a body must deform non-reciprocally to have net translation after one period of articulation. Non-reciprocal motion is not time-invariant and is distinct when viewed for-

wards and backward in time. It was named after the motion of an idealized scallop, which can only open and close about a single hinge. After one cycle of opening and closing, the scallop returns to its original position due to the time-reversible hydrodynamics. Purcell stated that at least two degrees of freedom must vary with some out-of-phase component to effect propulsion. More recent work by Chambrion & Munnier [46] revealed a more general requirement of self-propulsion that relied on geometric arguments instead of time-reversibility. They showed that net motion is possible when a linear mapping of the shape (deformational) variables to another linear space result in an open path and also proved the same principle holds in the inviscid regime.

Before we investigate collective behavior, we begin by studying the motion of a basic swimmer model. In Ch. 2, we present the physical and mathematical details necessary to derive the equations of motion for a collection of swimmers. We then derive a simple, internally constrained inviscid swimmer in Ch. 3 and compare the results with the well-known Stokes flow solution [2, 4, 47].

References

1. Golestanian, R. Phoretic Active Matter. *arXiv preprint arXiv:1909.03747* (2019).
2. Najafi, A. & Golestanian, R. Simple swimmer at low Reynolds number: Three linked spheres. *Physical Review E* **69,** 062901 (2004).
3. Saffman, P. The self-propulsion of a deformable body in a perfect fluid. *Journal of Fluid Mechanics* **28,** 385–389 (1967).
4. Swan, J. W., Brady, J. F., Moore, R. S. & 174, C. Modeling hydrodynamic self-propulsion with Stokesian Dynamics. Or teaching Stokesian Dynamics to swim. *Physics of Fluids* **23,** 071901 (2011).
5. Lighthill, S. J. *Mathematical biofluiddynamics* (SIAM, 1975).
6. Ishihara, A., Segall, J. E., Block, S. M. & Berg, H. C. Coordination of flagella on filamentous cells of Escherichia coli. *Journal of Bacteriology* **155,** 228–237 (1983).
7. Wu, K. J. Fish Use Physics to Avoid Running into Each Other. *Nova.* `https://www.pbs.org/wgbh/nova/article/fish-use-physics-avoid-collisions/` (2019).
8. Copeland, M. F. & Weibel, D. B. Bacterial swarming: a model system for studying dynamic self-assembly. *Soft matter* **5,** 1174–1187 (2009).

9. Palacci, J. *et al.* Light-activated self-propelled colloids. *Philosophical Transactions of the Royal Society A: Mathematical, Physical and Engineering Sciences* **372,** 20130372 (2014).

10. Zhang, J., Grzybowski, B. A. & Granick, S. Janus particle synthesis, assembly, and application. *Langmuir* **33,** 6964–6977 (2017).

11. Howse, J. R. *et al.* Self-motile colloidal particles: from directed propulsion to random walk. *Physical review letters* **99,** 048102 (2007).

12. Buttinoni, I., Volpe, G., Kümmel, F., Volpe, G. & Bechinger, C. Active Brownian motion tunable by light. *Journal of Physics: Condensed Matter* **24,** 284129 (2012).

13. Reynolds, O. XXIX. An experimental investigation of the circumstances which determine whether the motion of water shall be direct or sinuous, and of the law of resistance in parallel channels. *Philosophical Transactions of the Royal society of London,* 935–982 (1883).

14. Batchelor, C. K. & Batchelor, G. *An introduction to fluid dynamics* (Cambridge university press, 2000).

15. Lamb, H. *Hydrodynamics* (University Press, 1924).

16. Taylor, G. I. Analysis of the swimming of microscopic organisms. *Proceedings of the Royal Society of London. Series A. Mathematical and Physical Sciences* **209,** 447–461 (1951).

17. Avron, J., Kenneth, O. & Oaknin, D. Pushmepullyou: an efficient microswimmer. *New Journal of Physics* **7,** 234 (2005).

18. Elgeti, J., Winkler, R. G. & Gompper, G. Physics of microswimmers—single particle motion and collective behavior: a review. *Reports on progress in physics* **78,** 056601 (2015).

19. Burkholder, E. W. *Single Particle Motion in Active Matter* PhD thesis (California Institute of Technology, 2019).

20. Pooley, C., Alexander, G. & Yeomans, J. Hydrodynamic interaction between two swimmers at low Reynolds number. *Physical review letters* **99,** 228103 (2007).

21. Lauga, E. & Bartolo, D. No many-scallop theorem: Collective locomotion of reciprocal swimmers. *Physical Review E* **78,** 030901 (2008).

22. Marchetti, M. C. *et al.* Hydrodynamics of soft active matter. *Reviews of Modern Physics* **85,** 1143 (2013).

23. Klotsa, D. As above, so below, and also in between: mesoscale active matter in fluids. *Soft matter* **15,** 8946–8950 (2019).

24. *NIST Chemistry WebBook* Online. 2020.

25. *Material paramters:* $\rho^{\text{air}} = 1.2\,\text{kg/m}^3$, $\rho^{\text{water}} = 1000\,\text{kg/m}^3$, $\mu^{\text{air}} = 2 \times 10^{-5}\,\text{Pa} * \text{s}$, $\mu^{\text{water}} = 1 \times 10^{-3}\,\text{Pa} * \text{s}$,

26. Verma, S., Novati, G. & Koumoutsakos, P. Efficient collective swimming by harnessing vortices through deep reinforcement learning. *Proceedings of the National Academy of Sciences* **115,** 5849–5854 (2018).

27. Vicsek, T., Czirók, A., Ben-Jacob, E., Cohen, I. & Shochet, O. Novel type of phase transition in a system of self-driven particles. *Physical review letters* **75,** 1226 (1995).

28. Hendrickx, J. & Blondel, V. *Convergence of different linear and non-linear Vicsek models* in *MTNS 2006* (2006).

29. Chaté, H., Ginelli, F., Grégoire, G., Peruani, F. & Raynaud, F. Modeling collective motion: variations on the Vicsek model. *The European Physical Journal B* **64,** 451–456 (2008).

30. Liu, Z. & Guo, L. Connectivity and synchronization of Vicsek model. *Science in China Series F: Information Sciences* **51,** 848–858 (2008).

31. Bolley, F., Cañizo, J. A. & Carrillo, J. A. Mean-field limit for the stochastic Vicsek model. *Applied Mathematics Letters* **25,** 339–343 (2012).

32. Kellogg, O. D. *Foundations of potential theory* (Courier Corporation, 1953).

33. Pozrikidis, C. & Jankowski, D. *Introduction to theoretical and computational fluid dynamics* (Oxford university press New York, 1997).

34. Techet, A. *Potential Flow Theory* 2005.

35. Yurkovetsky, Y. & Brady, J. F. Statistical mechanics of bubbly liquids. *Physics of Fluids* **8,** 881–895 (1996).

36. Kanso, E., Marsden, J. E., Rowley, C. W. & Melli-Huber, J. B. Locomotion of articulated bodies in a perfect fluid. *Journal of Nonlinear Science* **15,** 255–289 (2005).

37. Wu, T. Hydromechanics of swimming propulsion. Part 1. Swimming of a two-dimensional flexible plate at variable forward speeds in an inviscid fluid. *Journal of Fluid Mechanics* **46,** 337–355 (1971).

38. Wu, T., Brokaw, C. J. & Brennen, C. *Swimming and flying in nature* (Springer, 1975).

39. Moore, D. The boundary layer on a spherical gas bubble. *Journal of Fluid Mechanics* **16,** 161–176 (1963).

40. Hinch, E. & Nitsche, L. C. Nonlinear drift interactions between fluctuating colloidal particles: oscillatory and stochastic motions. *Journal of Fluid Mechanics* **256,** 343–401 (1993).

41. Goldstein, H., Poole, C. & Safko, J. *Classical mechanics* (American Association of Physics Teachers, 2002).

42. Minguzzi, E. Rayleigh's dissipation function at work. *European Journal of Physics* **36,** 035014 (2015).

43. Kanso, E. & Marsden, J. E. *Optimal motion of an articulated body in a perfect fluid* in *Proceedings of the 44th IEEE Conference on Decision and Control* (2005), 2511–2516.

44. Kanso, E. Swimming in an inviscid fluid. *Theoretical and Computational Fluid Dynamics* **24,** 201–207 (2010).

45. Purcell, E. M. Life at low Reynolds number. *American journal of physics* **45,** 3–11 (1977).

46. Munnier, A. & Chambrion, T. Generalized scallop theorem for linear swimmers. *arXiv* (2010).

47. Golestanian, R. & Ajdari, A. Analytic results for the three-sphere swimmer at low Reynolds number. *Physical Review E* **77,** 036308 (2008).

Chapter 2

POTENTIAL FLOW THEORY

In this chapter, we present the theoretical developments required to derive the equations of motion for bodies in a potential fluid using a Lagrangian framework. Both potential flow and Lagrangian mechanics can model arbitrary body geometry and deformation, but we focus on collections of rigid spheres as this makes analytical progress easier. We begin by reviewing the differential equations and boundary conditions for potential flow. The Lagrangian for the fluid and particles is then calculated. We derive the particle equations of motion and highlight the interesting aspects of the hydrodynamic interactions. The inviscid approximation is relaxed, and bulk viscous forces are also derived using the Rayleigh dissipation theorem.

2.1 Fluid Domain

We model the bulk fluid at an infinite Reynolds number such that viscous forces can be neglected. The Navier-Stokes equations are then reduced to the Euler equations where inertia and pressure forces directly balance

$$\rho\left(\frac{\partial \boldsymbol{u}}{\partial t}+\boldsymbol{u}\cdot\nabla\boldsymbol{u}\right)=-\nabla p\ . \tag{2.1}$$

Unfortunately, the Euler equations still contain the non-linear inertia convection term. By neglecting interfacial boundary layers and wakes, we approximate the flow as irrotational, which allows the use of potential flow theory [1, 2]. The fluid velocity can then be written as the gradient of a scalar potential

$$\boldsymbol{u}=\nabla\phi\ . \tag{2.2}$$

Substitution of ϕ into the equation of continuity (mass conservation) for an incompressible fluid results in Laplace's equation at all points in the fluid domain

$$\nabla^2\phi=0\ . \tag{2.3}$$

No flux boundary conditions are enforced on all particle surfaces $\partial\Omega_\alpha$ as

$$\nabla\phi|_{\partial\Omega_\alpha}\cdot\boldsymbol{n}=\boldsymbol{U}_\alpha\cdot\boldsymbol{n}\ , \tag{2.4}$$

where $\boldsymbol{n}$ is the unitary outward pointing normal (from the particle into the fluid) and $\boldsymbol{U}_\alpha$ is the translational velocity of particle α, as shown in Fig. 2.1. We cannot enforce no-slip boundary conditions on particle surfaces, as only

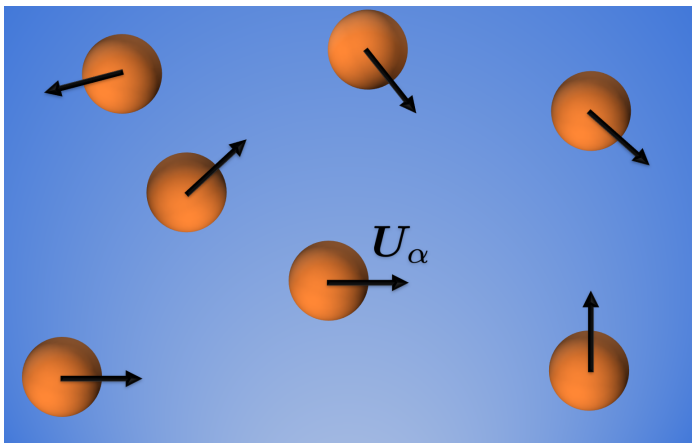

Figure 2.1: Spherical particles α of radius a with translational velocities $\boldsymbol{U}_\alpha$.

two scalar boundary conditions can be given for Laplace's equation (Eq. (2.3)). Since we are only concerned with the normal direction of the velocity, the rotational motion of the spherical particles (and their corresponding torque) is inconsequential due to the spherical isotropy. Particle rotation can be added to the boundary conditions for non-isotropic shapes if desired.

Infinitely far from the particles, we assume the fluid is at rest such that the potential decays to an arbitrary reference value, which we set to zero

$$\phi(\,|\boldsymbol{x}| \to \infty) = 0\ . \tag{2.5}$$

We turn to Lagrangian mechanics to determine the particle equations of motion. The advantage of Lagrangian mechanics is only scalar total energies must be derived, whereas the vector forces on all particles must be explicitly derived in Newtonian mechanics. We assume no external fields are acting on the fluid (i.e. $\mathscr{V}^{(\mathrm{f})} = 0$) such that the fluid Lagrangian is equal to the kinetic energy $\mathscr{L}^{(\mathrm{f})} = \mathscr{T}^{(\mathrm{f})}$. For constant mass density (incompressible fluid), the fluid kinetic energy is given by the integral of the local kinetic energy density over the fluid domain

$$\mathscr{T}^{(\mathrm{f})} = \frac{1}{2}\,\rho \int u^2(\boldsymbol{x})\, dV\ . \tag{2.6}$$

The integrand is then recast using potential flow theory as $u^2 = \nabla\phi \cdot \nabla\phi$. Further manipulation and application of the divergence theorem to relate the potential gradient to the boundary conditions of all N particles results in

$$\mathscr{T}^{(\mathrm{f})} = -\frac{1}{2}\rho \sum_{\alpha=1}^{N} \left(\int_{\partial\Omega_\alpha} \phi\, \boldsymbol{n}\, dS \right) \cdot \boldsymbol{U}_\alpha \ . \tag{2.7}$$

The negative sign in Eq. (2.7) is due to the convention of the normal vector pointing into the fluid domain from the solid—established by the no flux boundary conditions in Eq. (2.4). As Laplace's equation (Eq. (2.3)) is linear, the solution must be linear in the particle velocity via the no flux boundary conditions

$$\phi\left(\boldsymbol{x}\right) = \sum_{\beta=1}^{N} \boldsymbol{\Phi}_\beta\left(\boldsymbol{x}; \{\boldsymbol{x} - \boldsymbol{R}_\beta\}\right) \cdot \boldsymbol{U}_\beta \ . \tag{2.8}$$

The center position of particle β is denoted by $\boldsymbol{R}_\beta$. The parametric configuration dependence on the potential solution must be true given the surface boundary conditions and their radially decaying potential disturbance. The potential solution $\boldsymbol{\Phi}$ is calculated via a multipole expansion about the spherical centers. A translating sphere creates a dipolar potential disturbance $O(r^{-2})$ at leading order [2, 3], and higher order polar moments can be neglected, as shown in Bonnecaze & Brady [4, 5].

Substitution of Eq. (2.8) into Eq. (2.7) simplifies the kinetic energy into a quadratic form of the particle velocities. Using Einstein summation convention on all repeated subscripts, the fluid kinetic energy is given by

$$\mathscr{T}^{(\mathrm{f})} = \frac{1}{2}\rho V\ \boldsymbol{U}_\beta \cdot \boldsymbol{M}_{\beta\alpha} \cdot \boldsymbol{U}_\alpha \ , \tag{2.9}$$

where the "added" mass tensor is defined as

$$\boldsymbol{M}_{\beta\alpha}(\{\boldsymbol{R}_\gamma\}) \coloneqq -\frac{1}{V} \int_{\partial\Omega_\alpha} \boldsymbol{\Phi}_\beta\, \boldsymbol{n}\, dS \ . \tag{2.10}$$

The volume of a spherical particle of radius a is $V = (4/3)\pi a^3$. Each added mass tensor element is dependent on the configuration of all $\boldsymbol{R}_\gamma$ particles in the system. The added mass tensor physically captures the effective increase in inertia that a particle (or pair of particles) experiences due to the interactions with all other particles. The source of the interesting phenomena we study is the configurational dependence of the added mass tensor. Note that as defined, the added mass tensor is dimensionless.

The added mass tensor is calculated via a Taylor expansion of the potential $\boldsymbol{\Phi}$ about particle center positions. The constant term in the expansion is zero by symmetry (the unit normal is an odd function over the spherical surface). Therefore, the added mass is proportional to the gradient of the dipolar potential at leading order, which is $O(r^{-3})$. Further details on the explicit calculation of added mass tensor can be found in App. A. An isolated dipolar sphere has an added mass of

$$\boldsymbol{M}^{(\text{isolated})} = \frac{1}{2}\mathbf{I} \,, \tag{2.11}$$

and the added mass that one sphere α of radius a experiences from dipole-dipole interactions with one other sphere β is

$$\boldsymbol{M}^{(\text{d-d})}_{\alpha\beta} = \frac{a^3}{2}\left(\frac{1}{|\boldsymbol{r}|^3}\,\mathbf{I} - \frac{3}{|\boldsymbol{r}|^5}\,\boldsymbol{r}\otimes\boldsymbol{r}\right) \,, \tag{2.12}$$

where $\boldsymbol{r} = \boldsymbol{R}_\alpha - \boldsymbol{R}_\beta$ and $\otimes$ denotes the outer (dyadic) product.

Finally, we can also simplify the vector notation of Eq. (2.9) by using a stacked vector of the individual particle velocity vectors ($\boldsymbol{U} = [\boldsymbol{U}_1, \boldsymbol{U}_2, \ldots, \boldsymbol{U}_N]^{\mathrm{T}}$) as

$$\mathscr{T}^{(\text{f})} = \frac{1}{2}\,\rho\, V\; \boldsymbol{U}\cdot\boldsymbol{M}\cdot\boldsymbol{U} \,. \tag{2.13}$$

The Lagrangian of the fluid is therefore wholly determined by the particle velocities and their configuration. We must now add the particles' real mass and potential energy to solve the Lagrangian of the entire system.

2.2 Solid Particles

In our systems, we model the bodies as collections of spheres possessing the same radii a and density $\rho^{(\text{p})}$. We can immediately define the kinetic energy of all particles in the canonical fashion

$$\mathscr{T}^{(\text{p})} = \frac{1}{2}\,\rho^{(\text{p})}\, V\; \boldsymbol{U}\cdot\boldsymbol{U} \,. \tag{2.14}$$

We can add an arbitrary conservative particle potential $\mathscr{V}^{(\text{p})}$, such as harmonic springs to connect particles or a WCA potential to prevent particle overlap. Non-conservative potentials can also be included through the Rayleigh dissipation function, as will be discussed in § 2.3. The total Lagrangian for the system is the sum of the constituent Lagrangians from the fluid and particles. Using Eqs. (2.13)–(2.14), the total Lagrangian is given as

$$\mathscr{L} = \mathscr{T} - \mathscr{V} = \frac{1}{2}\,V\,\boldsymbol{U}\cdot(\rho\,\boldsymbol{M} + \rho^{(\text{p})}\,\mathbf{I})\cdot\boldsymbol{U} \;-\; \mathscr{V}^{(\text{p})} \,. \tag{2.15}$$

Lagrange's equation of motion conserves energy via the principle of least action and is given as

$$\frac{d}{dt}\left(\frac{\partial \mathscr{L}}{\partial \dot{\boldsymbol{R}}}\right) - \frac{\partial \mathscr{L}}{\partial \boldsymbol{R}} = 0 \ . \tag{2.16}$$

The equation of motion for each particle dimension is then

$$\rho V \left(M_{kj} + \frac{\rho^{(\mathrm{p})}}{\rho}\,\delta_{kj}\right)\dot{U}_j - \rho\, V \left(\frac{1}{2} U_i \frac{\partial M_{ij}}{\partial R_k}\, U_j - \frac{\partial M_{kj}}{\partial R_i}\, U_i\, U_j\right) = -\frac{\partial \mathscr{V}^{(\mathrm{p})}}{\partial R_k} \ . \tag{2.17}$$

Note that repeated Roman indices also imply Einstein summation convention. In this study, we use two separate but interrelated indices. Greek indices α, β, γ account for particle number, and each contain 3 entries (x, y, z Cartesian coordinates). Roman indices i, j, k are the absolute index number, and each contains one entry. This implies that $\boldsymbol{M}_{\alpha\beta}$ is a 3×3 tensor, whereas M_{ij} is a scalar.

The configuration-dependent added mass must be a source of self-propulsion in the potential regime. If the added mass was independent of the particle configuration, the equations of motion immediately reduce Newton's equations for constant mass particles

$$\mathscr{M}_{kj}\,\dot{U}_j = -\frac{\partial \mathscr{V}^{(\mathrm{p})}}{\partial R_k} \ , \tag{2.18}$$

and self-propulsion would not be possible by only varying the particle configuration. We have defined the "total" mass tensor as

$$\mathscr{M}_{kj} = \rho\, V \left(M_{kj} + \frac{\rho^{(\mathrm{p})}}{\rho}\ \delta_{kj}\right) \ , \tag{2.19}$$

and denote the Kronecker delta δ_{kj}. For simplicity, we denote the ratio of mass densities as $\Gamma = \rho^{(\mathrm{p})}/\rho$ and the fluid mass displaced by a single sphere as $\nu = \rho\, V$ so that the mass tensor is more compactly written

$$\mathscr{M}_{kj} = \nu\,(M_{kj} + \Gamma\ \delta_{kj}) \ . \tag{2.20}$$

The importance of the configuration-dependent added mass can also be seen from the hydrodynamic forces directly. Hinch & Nitsche [6] proved that the hydrodynamic pressure forces (exerted by the fluid on the particles) can be related to the fluid kinetic energy terms in Lagrange's equation (Eq. (2.16))

$$\mathbf{F}^{\mathrm{P}} = -\frac{d}{dt}\left(\frac{\partial \mathscr{T}^{(\mathrm{f})}}{\partial \dot{\boldsymbol{R}}}\right) + \frac{\partial \mathscr{T}^{(\mathrm{f})}}{\partial \boldsymbol{R}} \ . \tag{2.21}$$

The particles then have two ways to interact hydrodynamically. They may either accelerate their surrounding fluid ($\dot{U}_k \neq 0$), or vary their relative positions to take advantage of the added mass tensor (cf. Eq. (2.13)). An isolated particle traveling at constant velocity consequently experiences no net hydrodynamic force, commonly referred to as D'Alembert's paradox [7].

We finally turn to the particle linear momentum in order to determine all canonical coordinates and define it as

$$\mathbf{P} \coloneqq \mathscr{M}\, \boldsymbol{U} \ . \tag{2.22}$$

The total linear momentum of the particles is then given by

$$\mathbf{P}^{(t)} = \sum_{\alpha=1}^{N} \mathbf{P}_\alpha \ , \tag{2.23}$$

and can be viewed as the impulse required from the fluid to accelerate all particles from rest to their current state. If the potential energy $\mathscr{V}^{(\mathrm{p})}$ is purely internal to the system, the Lagrangian will only depend on relative configuration and not absolute particle positions. This implies that the Lagrangian must be invariant to a rigid spatial translation of the entire system (i.e. $\sum_\alpha \frac{\partial \mathscr{L}}{\partial \boldsymbol{R}_\alpha} = \mathbf{0}$). Lagrange's equation of motion (Eq. (2.16)) then reduces to $\dot{\mathbf{P}}^{(t)} = 0$. We now have two conserved quantities in potential flow: total energy $\mathscr{T} + \mathscr{V}$ and total linear momentum $\mathbf{P}^{(t)}$ [8]. The total energy is also known as the Hamiltonian $\mathscr{H} = \mathscr{T} + \mathscr{V}$, and its conservation allows the application of equilibrium statistical mechanics, as Yurkovetsky & Brady did in bubbly liquids [3]. With a Hamiltonian, the collection of particles can be treated as a canonical ensemble, a partition function can be defined, and thermodynamic phase behavior can then be analyzed.

2.3 Viscous Dissipation

Potential flow theory only requires that the fluid velocity field is irrotational and incompressible. We can therefore apply the Rayleigh dissipation function [9, 10] to the Lagrangian framework and derive the effective bulk viscous dissipation inherent in a finite Reynolds flow. The viscous dissipation is derived via a balance of energy and is given by

$$\dot{\mathrm{E}}^{\mathrm{v}} = 2\,\mu \int \mathbf{e} : \mathbf{e}\ dV \ , \tag{2.24}$$

where superscript v denotes viscous effects and is not an index. The symmetric rate of strain tensor $\mathbf{e}$ double contraction can be rewritten in terms of the scalar potential as

$$\dot{\mathrm{E}}^{\mathrm{v}} = 2\,\mu \int \nabla\nabla\phi : \nabla\nabla\phi \; dV \; . \tag{2.25}$$

From linearity of Laplace's equation, we can derive a quadratic form of the dissipation in the particle velocities

$$\dot{\mathrm{E}}^{\mathrm{v}} = \boldsymbol{U} \cdot \boldsymbol{\mathcal{R}} \cdot \boldsymbol{U} \; , \tag{2.26}$$

where we group the remaining integral and constants into the Rayleigh dissipation tensor $\boldsymbol{\mathcal{R}}$ (see App. B for further details). Analogous to the added mass tensor, the Rayleigh dissipation tensor is purely a function of geometry and configuration. By the Rayleigh dissipation function, the viscous dissipative force can then be calculated via the velocity derivative as

$$\mathbf{F}^{\mathrm{v}} = -\frac{1}{2}\frac{\partial \dot{\mathrm{E}}^{\mathrm{v}}}{\partial \boldsymbol{U}} = -\boldsymbol{\mathcal{R}} \cdot \boldsymbol{U} \; . \tag{2.27}$$

An isolated sphere experiences a drag force of $\mathbf{F}^{\mathrm{v}} = -12\,\pi\,a\,\mu\,\boldsymbol{U}$. We can then directly add the viscous dissipation to Eq. (2.16)

$$\mathbf{F}^{\mathrm{v}} = \frac{d}{dt}\left(\frac{\partial \mathscr{L}}{\partial \dot{\boldsymbol{R}}}\right) - \frac{\partial \mathscr{L}}{\partial \boldsymbol{R}} \; , \tag{2.28}$$

as shown in Goldstein §1.5 [9].

References

1. Techet, A. *Potential Flow Theory* 2005.
2. Batchelor, C. K. & Batchelor, G. *An introduction to fluid dynamics* (Cambridge university press, 2000).
3. Yurkovetsky, Y. & Brady, J. F. Statistical mechanics of bubbly liquids. *Physics of Fluids* **8,** 881–895 (1996).
4. Bonnecaze, R. & Brady, J. A method for determining the effective conductivity of dispersions of particles. *Proceedings of the Royal Society of London. Series A: Mathematical and Physical Sciences* **430,** 285–313 (1990).
5. Bonnecaze, R. & Brady, J. The effective conductivity of random suspensions of spherical particles. *Proceedings of the Royal Society of London. Series A: Mathematical and Physical Sciences* **432,** 445–465 (1991).
6. Hinch, E. & Nitsche, L. C. Nonlinear drift interactions between fluctuating colloidal particles: oscillatory and stochastic motions. *Journal of Fluid Mechanics* **256,** 343–401 (1993).

7. d'Alembert, J. L. R. *Essai d'une nouvelle théorie de la résistance des fluides* (David l'ainé, 1752).

8. Lamb, H. *Hydrodynamics* (University Press, 1924).

9. Goldstein, H., Poole, C. & Safko, J. *Classical mechanics* (American Association of Physics Teachers, 2002).

10. Minguzzi, E. Rayleigh's dissipation function at work. *European Journal of Physics* **36,** 035014 (2015).

Chapter 3

COLLINEAR SWIMMER

Saffman first demonstrated inviscid self-propulsion [1], and we wish to construct a minimal body capable of self-propulsion within our framework. We chose to follow a prototypical Stokes swimmer design [2], as we thought it would be a good example and allow comparison between Stokes and inviscid swimming. The swimmer consists of three identical spheres connected via two "arms" (Fig. 3.1). The arms are thin, such that we can neglect them hydrodynamically. The body is referred to as a "swimmer" because after a period of articulation, the body is prescribed to return to its original configuration. Therefore, if there is any net translation (self-propulsion) after one complete period, the same propulsion will occur for all future periods by symmetry.

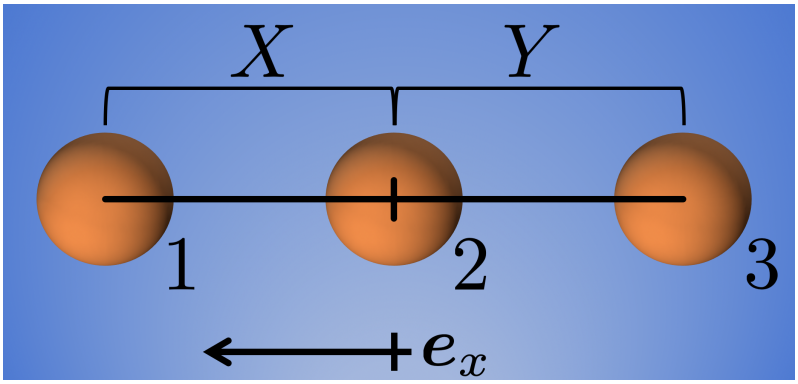

Figure 3.1: A swimmer: Three spheres of equal radius a and density connected by thin arms with prescribed deformation. The swimmer is collinear such that it only translates along one spatial dimension.

The spheres have spatial center positions $\{R_1, R_2, R_3\}$, which can be linearly mapped to a set of generalized "body" coordinates $\{X, Y, Z\}$. The relative separation between neighboring particle pairs is denoted as X and Y, which will be the two internal degrees of freedom required for self-propulsion by the generalized scallop theorem [3, 4]. The body center of mass is called Z and will be tracked to determine the self-propulsion behavior of the swimmer. The

linear mappings for positional coordinates are given as

$$\begin{aligned} X &= R_2 - R_1 \ , \\ Y &= R_3 - R_2 \ , \text{ and} \\ Z &= \tfrac{1}{3}\left(R_1 + R_2 + R_3\right) \ . \end{aligned} \tag{3.1}$$

Analogous mappings can be defined for the velocity and acceleration components.

3.1 Translating Potential Swimmer

We only analyze the x-components of the mass tensors and kinematics as the y and z-axes can be neglected by symmetry. With no external forcing and momentum-free initial conditions, the total linear momentum of the body center of mass must be zero for all time ($P_z = 0$). In body coordinates, this conservation statement implies

$$\dot{Z} = -\frac{\mathscr{M}_{xz}}{\mathscr{M}_{zz}}\,\dot{X} - \frac{\mathscr{M}_{yz}}{\mathscr{M}_{zz}}\,\dot{Y} \ . \tag{3.2}$$

For the swimmer to translate on net after one period of articulation, it is required that the time average of $\dot{Z}$ be non-zero. As the total mass tensor is only defined in terms of the relative particle coordinates, we must determine the body coordinate mass tensor entries by setting the total linear momentum equal to zero (Eq. (2.23)), substituting the body coordinate velocity mappings, and defining effective body mass from the resulting balance as

$$\begin{aligned} \mathscr{M}_{xz} &= \tfrac{1}{3}\left(-2\,\mathscr{M}_{11} + \mathscr{M}_{22} + \mathscr{M}_{33} - \mathscr{M}_{12} + 2\,\mathscr{M}_{23} - \mathscr{M}_{13}\right) \ , \\ \mathscr{M}_{yz} &= \tfrac{1}{3}\left(-\mathscr{M}_{11} - \mathscr{M}_{22} + 2\,\mathscr{M}_{33} - 2\,\mathscr{M}_{12} + \mathscr{M}_{23} + 2\,\mathscr{M}_{13}\right) \ , \text{ and} \\ \mathscr{M}_{zz} &= \mathscr{M}_{11} + \mathscr{M}_{22} + \mathscr{M}_{33} + 2\,\mathscr{M}_{12} + 2\,\mathscr{M}_{23} + 2\,\mathscr{M}_{13} \ . \end{aligned} \tag{3.3}$$

Interestingly, $\mathscr{M}_{xz}$ and $\mathscr{M}_{yz}$ are not dependent on the real mass for our swimmer model. The real mass is only found on the diagonal total mass tensor entries ($\mathscr{M}_{11}$, $\mathscr{M}_{22}$, $\mathscr{M}_{33}$), and is canceled out by the addition and subtraction operations. If the spheres instead had distinct masses, $\mathscr{M}_{xz}$ and $\mathscr{M}_{yz}$ would have a real mass component and be weighted according to the given model. In order to study the evolution of $\dot{Z}$, we prescribe the internal velocity degrees of freedom $\dot{X}$ and $\dot{Y}$ as

$$\begin{aligned} \dot{X} &= U_0 \cos\left(\omega\, t\right) \ , \\ \dot{Y} &= U_0 \cos\left(\omega\, t + \delta\right) \ . \end{aligned} \tag{3.4}$$

We are interested in the center of mass displacement after one period, which is given by the time integral of Eq. (3.2)

$$\Delta Z\left(t=2\pi/\omega\right)=-\int_0^{2\pi/\omega}\left(\frac{\mathscr{M}_{xz}}{\mathscr{M}_{zz}}\dot{X}+\frac{\mathscr{M}_{yz}}{\mathscr{M}_{zz}}\dot{Y}\right)\,dt\;. \tag{3.5}$$

Note that if the mass tensor elements are not a function of configuration, the mass tensor elements can be removed from the integral, and the integral of a cosine wave over one period is identically zero. Thus, the added mass due to hydrodynamic interactions must be the source of self-propulsion for the swimmer being studied.

Small Amplitude Motion

Assuming that the particle oscillations are small compared to their average separation, $\epsilon=\left(U_0/\omega\right)/|X_0|\ll 1$, we can Taylor expand the mass tensor elements about the average separation $(X_0,\,Y_0)$. Integration of the leading order Taylor expansion reveals that only the cross-terms (having both X and Y coordinates in the integrand) are non-zero due to simple trigonometric identities. The leading order Taylor expansion of Eq. (3.2) is calculated as

$$\Delta\tilde{Z}=\pi\,\sin\delta\left(\frac{U_0}{a\,\omega}\right)^2\left(\frac{\partial}{\partial\tilde{X}}\left(\frac{\mathscr{M}_{yz}}{\mathscr{M}_{zz}}\right)\bigg|_{\tilde{X}_0,\tilde{Y}_0}-\frac{\partial}{\partial\tilde{Y}}\left(\frac{\mathscr{M}_{xz}}{\mathscr{M}_{zz}}\right)\bigg|_{\tilde{X}_0,\tilde{Y}_0}\right)\;, \tag{3.6}$$

where we have non-dimensionalized the length scales by the spherical radius a and denote dimensionless quantities with a tilde. Self-propulsion ($\Delta\tilde{Z}\neq 0$) is therefore dependent on both the kinematics and configuration. To have a net translation, there must be a phase shift between the oscillators ($\delta\neq c\,\pi$ for integer c) and the effective mass tensor element variations must not cancel. The relative center of mass translation is governed by the competition of two length (or time) scales: one set by geometry, and another set by the system kinematics, which is tuneable

$$\frac{\mathrm{L}_{\mathrm{dyn}}}{\mathrm{L}_{\mathrm{geo}}}=\frac{U_0/\omega}{a}\;,\qquad\qquad\frac{\tau_{\mathrm{osc}}}{\tau_{\mathrm{trans}}}=\frac{1/\omega}{a/U_0}\;. \tag{3.7}$$

Increasing the translational amplitude of oscillations increases the value of the dynamic length scale and leads to higher relative motion. Derivatives are then calculated and evaluated for the special case of equispaced particles $R_0=-X_0=-Y_0$. For neutrally buoyant swimmers ($\Gamma=1$), Eq. (3.6) becomes

$$\Delta\tilde{Z}=\pi\,\sin\delta\left(\frac{U_0}{a\,\omega}\right)^2\frac{36\,\left(744\,R_0^9-1564\,R_0^6+1632\,R_0^3-1045\right)}{R_0(144\,R_0^6-204\,R_0^3+209)^2}\;. \tag{3.8}$$

Importantly, the dimensionless displacement scales as $O(R_0^{-4})$ to leading order, which is expected from the derivative of the added mass tensor. Note that the dimensionless spacing must be greater than two to be physical (no particle overlap). For a configuration with maximized phase difference $\delta = \pi/2$, we plot the body center of mass displacement over one period of articulation in Fig. 3.2 (blue curve). Note that in general, both the magnitude and sign of

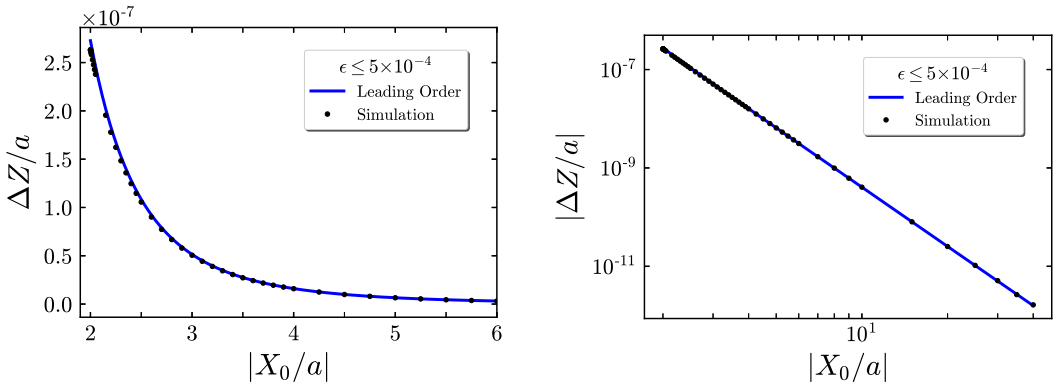

Figure 3.2: Relative displacement (a) and log-log relative displacement (b) for one period of articulation with $X_0 = Y_0$, $\Gamma = 1$, $\delta = \pi/2$. Blue curve from Eq. (3.8) and black points depict numerical simulation results.

the resultant displacement will vary depending on the value of the phase angle δ. A phase difference of $\pi/2$ corresponds to the 1–2 particle pair initially at its equilibrium length and contracting with velocity $-U_0$ while the 2–3 pair is at rest in its minimum extensional length (cf. Eq. (3.4)). This phase difference results in the movement towards the positive x-axis (particle 1). If the phase difference is an integer multiple of π, no translation is possible at leading order, regardless of the internal mechanics.

It is important to note that the net motion of the internally constrained collinear swimmer—or indeed any similar swimmer in an inviscid, irrotational fluid—is still energetically conservative over a period of articulation. The prescribed kinematic constraints (Eq. (3.4)) must be upheld by a corresponding constraint force that the connecting arms provide. The work done by the constraint force over a period is given as the difference between the total kinetic energy at the beginning and end of the period, as shown in App. C. Since $\dot{X}$ and $\dot{Y}$ are periodic and the total linear momentum of the system must be zero for all times, the kinetic energy at the beginning and end of the articula-

tion period are the same. The work done by the constraint force on the body over one period is therefore identically zero, and the motion does not lead to dissipation.

Numerical Solution

In order to ascertain the validity of the leading order expansion, we numerically integrate $\dot{Z}$ (Eq. (3.2)). The initial positions of the particles were determined by integration of Eqs. (3.4), setting the central sphere to be placed at the origin, and specifying an average separation $R_0 = -X_0 = -Y_0$. Initial accelerations were set by the time derivatives of the velocity constraints and closed with a force-free condition on the overall swimmer. The simulation results had an approximately $O(R_0^{-4})$ center of mass translation decay, which was expected from the Taylor expansion (Fig. 3.2b). The full numerical solution shows excellent agreement with the leading order approximation (Fig. 3.2a).

When ϵ grows, the Taylor expansion will become less accurate as depicted in Fig. 3.3. Note that as defined $\epsilon \leq \frac{1}{2}$ to prevent particle overlap. As the

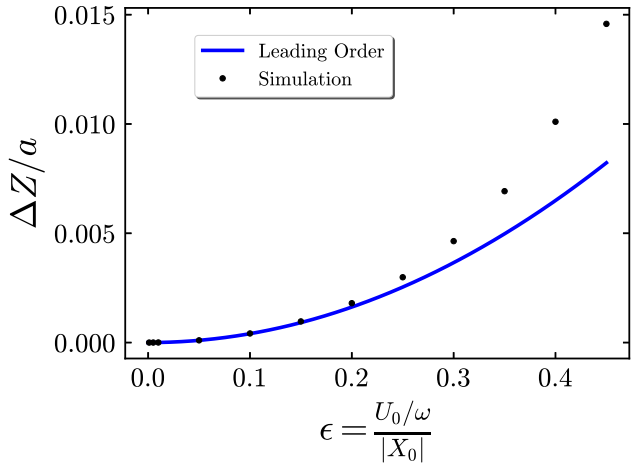

Figure 3.3: Relative displacement for one period of articulation with $X_0 = Y_0$, $\Gamma = 1$, $\delta = \pi/2$, $R_0 = 10$. Blue curve from Eq. (3.8) and black points depict numerical simulation results.

oscillations become larger in magnitude, the particles become significantly closer together at minimum separation and experience larger hydrodynamic interactions. The inverse cubic scaling of the hydrodynamic interactions causes

the closer interactions to overcompensate for the weaker interactions when the particles are at maximum separation and lead to a non-linear increase in displacement after one period.

Constant Center of Total Mass Approximation

As mentioned previously, the swimmer is able to self-propel due to the configuration dependence of the total mass tensor elements. If we assume that the particles are well separated, we can approximate $\mathscr{M}_{zz}$ as constant, as it is dependent on the real mass at leading order, and simplify Eq. (3.6)

$$\Delta\tilde{Z} = \left(\frac{U_0}{a\,\omega}\right)^2 \left[\frac{\pi\,\sin\delta}{\mathscr{M}_{zz}}\left(\frac{\partial\mathscr{M}_{yz}}{\partial\tilde{X}} - \frac{\partial\mathscr{M}_{xz}}{\partial\tilde{Y}}\right)\right]\Bigg|_{\tilde{X}_0,\tilde{Y}_0} . \tag{3.9}$$

Evaluation of the simplified equation for equispaced particles results in

$$\Delta\tilde{Z} = \pi\,\sin\delta\left(\frac{U_0}{a\,\omega}\right)^2\left(\frac{186\,R_0^3 - 187}{144\,R_0^7}\right) , \tag{3.10}$$

which possesses the same asymptotic $O(R_0^{-4})$ scaling as the leading order expansion (cf. Eq. (3.8)). We directly compare the leading order analytical solution to the constant center of mass solution in Fig. 3.4. The solutions differ

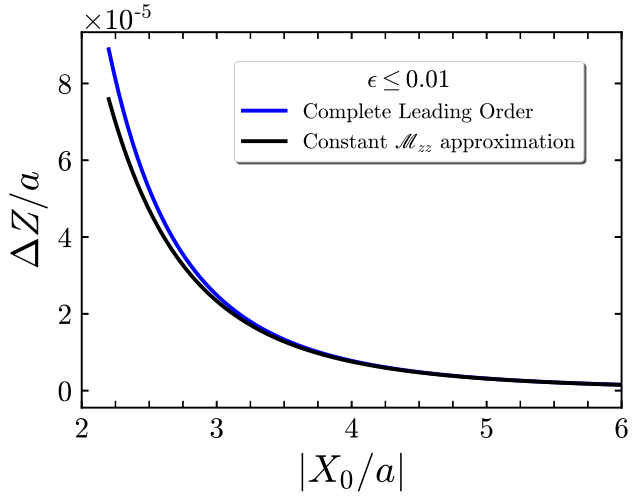

Figure 3.4: Relative displacement for one period of articulation with $X_0 = Y_0$, $\Gamma = 1$, $\delta = \pi/2$, Blue curve from Eq. (3.8) and black curve from Eq. (3.10).

only as the particle pair average separation becomes $O(3)$ and converge for well-separated particles, as expected. The direct coupling of the added mass $\mathscr{M}_{xz}$ and $\mathscr{M}_{yz}$ through the internal degrees of freedom is clearly a key source of self-propulsion for the swimmer presented.

3.2 Translating Stokes Swimmer

The Stokes regime is defined as $\mathrm{Re} \ll 1$ and inertial forces are negligible. The solutions to the Stokes flow hydrodynamics are well-known and can be found in Refs. [5, 6]. The Stokes hydrodynamic force is linear in the particle velocities and is written as

$$\mathbf{F}^{\mathrm{H}} = -\hat{\mathbf{R}} \cdot \boldsymbol{U} \ . \tag{3.11}$$

The hydrodynamic resistance tensor $\hat{\mathbf{R}}$ is only a function of the particle configuration, analogous to the added mass tensor in potential flow. Importantly, the translating sphere Stokes fluid disturbance scales as a monopole at leading order [5], which is a much longer-ranged interaction than in the potential fluid. We numerically simulate the Stokes hydrodynamics using the Stokesian Dynamics framework [7, 8]. A brief overview of Stokesian Dynamics can be found in App. D.

The translating Stokes swimmer is defined identically to the translating potential swimmer, with the same coordinate system (Eqs. (3.1)) and imposed velocity constraints (Eq. (3.4)). The system of equations governing motion in the Stokes regime is closed through a force-free condition on the overall swimmer. These conditions result in the Stokes swimmer center of mass velocity as

$$\dot{Z} = -\frac{\hat{\mathrm{R}}_{xz}}{\hat{\mathrm{R}}_{zz}}\,\dot{X} \ - \ \frac{\hat{\mathrm{R}}_{yz}}{\hat{\mathrm{R}}_{zz}}\,\dot{Y} \ . \tag{3.12}$$

Note that the Stokes equation of motion is analogous to the respective inviscid equation (cf. Eq. (3.2)) with the resistance tensor taking the place of the total mass tensor. As the resistance tensor is only a function of the particle configuration, the center of mass translation derivation is the same as in the inviscid regime, resulting in

$$\Delta\tilde{Z} = \pi \, \sin\delta \left(\frac{U_0}{a\,\omega}\right)^2 \left(\frac{\partial}{\partial \tilde{X}} \left(\frac{\hat{\mathrm{R}}_{yz}}{\hat{\mathrm{R}}_{zz}} \right) \bigg|_{\tilde{X}_0,\tilde{Y}_0} \ - \ \frac{\partial}{\partial \tilde{Y}} \left(\frac{\hat{\mathrm{R}}_{xz}}{\hat{\mathrm{R}}_{zz}} \right) \bigg|_{\tilde{X}_0,\tilde{Y}_0} \right) \tag{3.13}$$

for one period of articulation. In the Stokes regime, the partial derivatives are evaluated numerically using Stokesian Dynamics code extended from Ref. [9]. For comparison with both the inviscid regime and earlier work on Stokes swimmers, we only include the far-field hydrodynamic interactions and not the singular, short-ranged lubrication forces.

Before numerical evaluation, however, we can already anticipate the asymptotic scaling of $\Delta\tilde{Z}$ for well-separated particle pairs. An isolated translating sphere creates a monopole hydrodynamic disturbance [7], and the derivative of the monopole scales as $O(R_0^{-2})$. We therefore expect an inverse quadratic decay of the center of mass translation for large particle separation, which is what we observe in Fig. 3.5a. Notably, the Stokes regime exhibits two separate propulsion regimes. The higher-order reflection interactions become prominent and cause the differing decay at moderate separations of $O(3)$ in Fig. 3.5a.

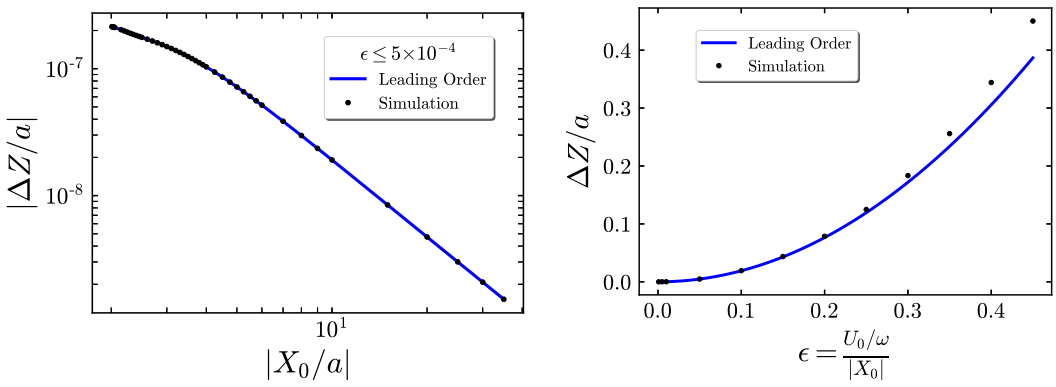

(a) (b)

Figure 3.5: The log-log relative displacement (a), and increasing small parameter ϵ (b) for one period of articulation with $X_0 = Y_0$, and $\delta = \pi/2$ ((b) $|X_0| = 10$). Blue curve from Eq. (3.13) and black points depict numerical simulation results.

As the relative oscillation amplitude ϵ grows, the numerical results again grow faster than the Taylor expansion (Fig. 3.5b) due to increased hydrodynamic interactions with non-linear scaling at near separation. However, the Taylor expansion is accurate for much larger values of ϵ than in the inviscid regime (cf. Fig. 3.5b). The leading order well-separated Stokes hydrodynamic interactions scale as $O(R_0^{-2})$, a much slower varying function compared to the leading order inviscid hydrodynamic interactions of $O(R_0^{-4})$. The smaller hydrodynamic variations lead to a more accurate approximation by using the interactions at the average separation.

Golestanian Swimmer

Najafi & Golestanian first proposed a similar three-sphere, collinear swimmer model [10] in the Stokes regime. The prescribed kinematics dictated that only one particle pair deformed at a time in a series of four discrete steps. The

swimmer starts out in its extended, equispaced configuration. During the first two steps, one arm contracts at a time to the same contracted length (i.e. $\dot{X} = \text{const}$, $\dot{Y} = 0$). The pairs then extend to their original length over the last two steps in the same order they contracted. The overall articulation is non-reciprocal and propels the swimmer on net. The swimmer model similarly predicted a quadratic scaling of the self-propulsion ΔZ (cf. Eq. (3.6)) with the relative oscillation amplitude ϵ.

A later study by Golestanian & Ajdari [2] focused on a swimmer with similar kinematic constraints to those presented in § 3.2 in which both particle pairs deformed sinusoidally. The continuously deforming swimmer also recovered the $\sin\delta$ translational dependence. They note that a general three-sphere swimmer must have a phase difference between the prescribed kinematics of the particle pairs, or self-propulsion will not occur.

In both works, Golestanian proves the magnitude of displacement is directly proportional to the area traced over a full cycle in configuration phase space. The integral for the translation magnitude (Eq. (3.5)) can be interpreted as the area swept out in $(\Delta X, \Delta Y)$ phase space. The original Golestanian swimmer [10] and the continuously deforming swimmer presented in this work trace out different shapes in configuration phase space. The Golestanian swimmer only moves one pair at a time, thereby tracing out a square over the articulation period (assuming the pairs deform identical lengths). The continuously deforming swimmer traces out an ellipse, and when the phase difference is maximized at $\delta = \pi/2$, the ellipse becomes a circle. Conversely, when the phase difference reaches an integer multiple of π, the ellipse collapses to a line, which encloses no area.

The side length of the square and the diameter of the circle are the same for identical swimmer oscillation amplitudes. By taking the ratio of the square to the circular area, we therefore predict the relative translation after one period of $\pi/4$ (continuously deforming: Golestanian [10]), which is the same ratio we recover numerically. We also recover the same ratio for identical swimmers in the potential flow regime, which is expected as it contains the same equation of motion (with $\hat{\mathrm{R}} \to \mathscr{M}$). However, the predicted ratio is only achieved for small amplitude oscillations ϵ. The phase space argument implicitly assumes that the hydrodynamic interactions are equivalent between the swimmers, which

becomes less accurate as the oscillation amplitude grows. The phase space argument for net-translation is powerful, as it makes a comparison between alternative swimmer designs easy for small amplitude oscillations.

3.3 Comparison Between Fluid Regimes

Now we arrive at the direct race between identical swimmers (continuous deformation) in inviscid and Stokes flow. We show the numerical solution for the center of mass translation after one period of oscillation in Fig. 3.6. As expected, the Stokes swimmer translates farther during the articulation period when the particles are well-separated. The strength of the interac-

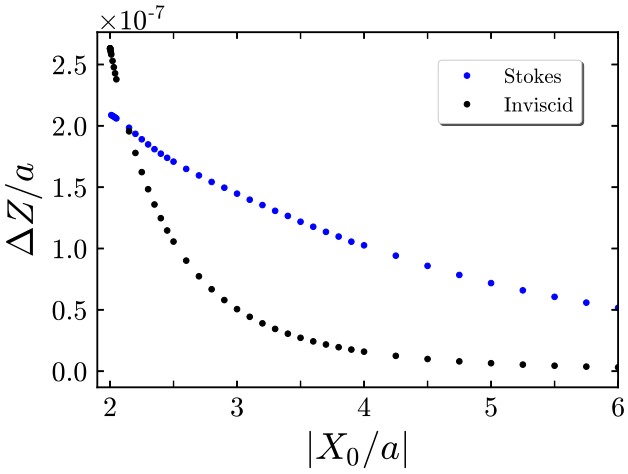

Figure 3.6: Comparison between identical swimmer center of mass translation in Stokes and inviscid fluids for one period of articulation with $X_0 = Y_0$, and $\delta = \pi/2$.

tions leading to self-propulsion is then proportional to the sensitivity of the coupling tensors with varying separation as well as their respective scaling (cf. Eqs. (3.2), (3.13)). As the Stokes regime possesses a much larger leading order interaction strength, the self-propulsion of the Stokes swimmer is consequently larger in magnitude for well-separated particle pairs. At narrow separations, the higher-order reflections in the Stokes case dominate and dampen the net translation.

References

1. Saffman, P. The self-propulsion of a deformable body in a perfect fluid. *Journal of Fluid Mechanics* **28,** 385–389 (1967).

2. Golestanian, R. & Ajdari, A. Analytic results for the three-sphere swimmer at low Reynolds number. *Physical Review E* **77,** 036308 (2008).

3. Purcell, E. M. Life at low Reynolds number. *American journal of physics* **45,** 3–11 (1977).

4. Munnier, A. & Chambrion, T. Generalized scallop theorem for linear swimmers. *arXiv* (2010).

5. Deen, W. M. *Analysis of transport phenomena* (Oxford University Press New York, 1998).

6. Happel, J. & Brenner, H. *Low Reynolds number hydrodynamics: with special applications to particulate media* (Springer Science & Business Media, 2012).

7. Durlofsky, L., Brady, J. F. & Bossis, G. Dynamic simulation of hydrodynamically interacting particles. *Journal of fluid mechanics* **180,** 21–49 (1987).

8. Brady, J. F. & Bossis, G. Stokesian dynamics. *Annual review of fluid mechanics* **20,** 111–157 (1988).

9. Swan, J. W., Brady, J. F., Moore, R. S. & 174, C. Modeling hydrodynamic self-propulsion with Stokesian Dynamics. Or teaching Stokesian Dynamics to swim. *Physics of Fluids* **23,** 071901 (2011).

10. Najafi, A. & Golestanian, R. Simple swimmer at low Reynolds number: Three linked spheres. *Physical Review E* **69,** 062901 (2004).

Appendix A

FURTHER DETAILS ON MASS TENSORS

Both the total mass tensor and its gradient with respect to particle centers are required for the full particle equations of motion given in the main text (Eq. (2.17)). We present the remaining details to derive the required quantities for both analysis and computation.

A.1 Added Mass Tensor

Calculation of the potential flow solution $\mathbf{\Phi}$ requires a multipole expansion of Laplace's equation (Eq. (2.3)). For constant volume particles, the monopole is identically zero, and the dipole captures the no-flux boundary condition. The hydrodynamic disturbances (velocity field) scale as the gradient of the potential, indicating the interactions between particles scale as $O(r^{-3})$, where r is the distance between their centers. Higher-order polar moments can be neglected, as shown in Bonnecaze & Brady [1, 2]. A detailed calculation of the mass tensor is found in Yurkovetsky & Brady [3].

The overall added mass tensor is symmetric and positive definite. The symmetry physically results from the tensor being a function of the absolute value of the distance between particles, so the added mass on particle one from particle two is the same as the reverse. The positive definite quality can be proved from the quadratic form of the fluid kinetic energy in the particle velocities (kinetic energy cannot be negative). The added mass tensor is calculated as a function of particle configuration with constituent tensors defined as

$$\boldsymbol{M} \coloneqq -\left(\mathbf{I} - \boldsymbol{M}^{(1)}\right)^{-1} \boldsymbol{M}^{(2)} \ . \tag{A.1}$$

Each 3×3 sub-tensor in $\boldsymbol{M}^{(1)}$ physically describes the dipole-dipole hydrodynamic interactions between a pair of particles, and the inversion operation represents the scattering of all hydrodynamic interactions. The second constituent mass tensor $\boldsymbol{M}^{(2)}$ can be directly calculated from $\boldsymbol{M}^{(1)}$ as

$$\boldsymbol{M}^{(2)} = -\boldsymbol{M}^{(1)} - \frac{1}{2}\mathbf{I} \ , \tag{A.2}$$

and is defined for notational convenience. The distance between particles α and β is the Euclidean norm, $|\boldsymbol{R}_{\alpha\beta}| = ||\boldsymbol{R}_\alpha - \boldsymbol{R}_\beta||_2$. Note that $|\boldsymbol{R}_{\alpha\beta}|$ is a scalar describing the distance between particles, not a second-order tensor. The first constituent added mass tensor is then defined as

$$\boldsymbol{M}^{(1)}_{\alpha\beta} \coloneqq -\frac{a^3}{2}\,\nabla_{\boldsymbol{y}}\,\nabla_{\boldsymbol{y}}\,|\boldsymbol{R}_{\alpha\beta}|^{-1} \tag{A.3}$$

for particle α different from particle β, where both particles are assumed to have constant spherical radius a. The gradients are with respect to the displacement between the pair as $\boldsymbol{y} = \boldsymbol{R}_\beta - \boldsymbol{R}_\alpha$. The second order gradient is then given explicitly by

$$\boldsymbol{M}^{(1)}_{\alpha\beta} = -\frac{a^3}{2}\left(\frac{3}{|\boldsymbol{R}_{\alpha\beta}|^5}\;\boldsymbol{R}_{\alpha\beta}\otimes\boldsymbol{R}_{\alpha\beta} - \frac{1}{|\boldsymbol{R}_{\alpha\beta}|^3}\;\mathbf{I}\right)\,, \tag{A.4}$$

where $\boldsymbol{R}_{\alpha\beta}$ is a shorthand for the relative displacement and not summed over. All 3×3 sub-tensors on the diagonal of $\boldsymbol{M}^{(1)}$ are the zero tensor.

A.2 Added Mass Tensor Gradient

The gradient of the mass tensor with respect to all particle centers $\boldsymbol{R}_\alpha$ is required for the particles' equations of motion. We denote the gradient of the added mass tensor first constituent with respect to the k-th dimension of particle centers as $M^{(1)}_{ij,k}$. The gradient particle introduces an anti-symmetry into the mathematics, as the tensor element is dependent on $\boldsymbol{R}_\alpha - \boldsymbol{R}_\beta$. Exploiting these symmetries yields the following simplifications to the calculation of the added mass tensor.

$$\boldsymbol{M}^{(1)}_{\alpha\beta,\alpha} = \boldsymbol{M}^{(1)}_{\beta\alpha,\alpha} = -\boldsymbol{M}^{(1)}_{\alpha\beta,\beta} = -\boldsymbol{M}^{(1)}_{\beta\alpha,\beta} \tag{A.5}$$

The repetition of indices in Eq. (A.5) does not imply Einstein summation convention, merely making explicit the fact that the gradient particle position coordinates must be one of the two particles in the mass tensor element. Each sub-tensor (size $3\times3\times3$) for the gradient mass tensor constituent one is given as

$$\begin{aligned}\left(M^{(1)}_{\alpha\beta,\gamma}\right)_{ijk} =&(\delta_{\alpha\gamma}-\delta_{\beta\gamma})\left(\frac{-3\,a^3}{2\,|\boldsymbol{R}_{\alpha\beta}|^5}\Big(\delta_{ij}\,(\boldsymbol{R}_{\alpha\beta})_k + \delta_{ik}\,(\boldsymbol{R}_{\alpha\beta})_j + \delta_{jk}\,(\boldsymbol{R}_{\alpha\beta})_i\Big)\right.\\ &\left.+\frac{15\,a^3}{2\,|\boldsymbol{R}_{\alpha\beta}|^7}\Big(\boldsymbol{R}_{\alpha\beta}\otimes\boldsymbol{R}_{\alpha\beta}\otimes\boldsymbol{R}_{\alpha\beta}\Big)_{ijk}\right)\,.\end{aligned} \tag{A.6}$$

The calculation of the full mass tensor gradient is complicated since a tensor, $\boldsymbol{A}$, must be computed numerically via tensor inversion $\boldsymbol{A} = \boldsymbol{B}^{-1} \coloneqq \left(\mathbf{I} - \boldsymbol{M}^{(1)}\right)^{-1}$. We therefore seek a closed-form equation for the gradient without calculating $\nabla \boldsymbol{B}$. We can avoid this issue by using the identity tensor to define $\nabla(\boldsymbol{B}^{-1})$ in terms of $\nabla \boldsymbol{B}$ and $\boldsymbol{B}^{-1}$ itself.

$$
\begin{aligned}
\delta_{ij} &= B_{ik}\, B^{-1}_{kj} \\
\frac{\partial}{\partial x_l}\Big(\delta_{ij}\Big) = 0 &= \frac{\partial B_{ik}}{\partial x_l}\, B^{-1}_{kj} + B_{ik}\, \frac{\partial B^{-1}_{kj}}{\partial x_l} \\
B_{ik}\, \frac{\partial B^{-1}_{kj}}{\partial x_l} &= -\frac{\partial B_{ik}}{\partial x_l}\, B^{-1}_{kj} \\
B^{-1}_{mi}\, B_{ik}\, \frac{\partial B^{-1}_{kj}}{\partial x_l} &= -B^{-1}_{mi}\, \frac{\partial B_{ik}}{\partial x_l}\, B^{-1}_{kj} \\
\delta_{mk}\, \frac{\partial B^{-1}_{kj}}{\partial x_l} &= -B^{-1}_{mi}\, \frac{\partial B_{ik}}{\partial x_l}\, B^{-1}_{kj} \\
\frac{\partial B^{-1}_{mj}}{\partial x_l} &= -B^{-1}_{mi}\, \frac{\partial B_{ik}}{\partial x_l}\, B^{-1}_{kj} \\
\nabla(\boldsymbol{B}^{-1}) &= -\boldsymbol{B}^{-1} \cdot \nabla \boldsymbol{B} \cdot \boldsymbol{B}^{-1}
\end{aligned}
\tag{A.7}
$$

Given $\nabla(\boldsymbol{B}^{-1})$, we can calculate the mass tensor gradient as

$$
\begin{aligned}
\frac{\partial M_{ij}}{\partial x_l} &= -\frac{\partial A_{ik}}{\partial x_l}\, M^{(2)}_{kj} - A_{ik}\, \frac{\partial M^{(2)}_{kj}}{\partial x_l} \\
&= A_{im}\, \frac{\partial B_{mn}}{\partial x_l}\, A_{nk}\, M^{(2)}_{kj} - A_{ik}\, \frac{\partial M^{(2)}_{kj}}{\partial x_l} \\
&= -A_{im}\, \frac{\partial M^{(1)}_{mn}}{\partial x_l} A_{nk} M^{(2)}_{kj} - A_{ik} \frac{\partial M^{(2)}_{kj}}{\partial x_l} \\
&= A_{im}\, \frac{\partial M^{(1)}_{mn}}{\partial x_l} M_{nj} + A_{ik}\, \frac{\partial M^{(1)}_{kj}}{\partial x_l} \\
&= A_{im} \left(\frac{\partial M^{(1)}_{mn}}{\partial x_l}\, M_{nj} + \frac{\partial M^{(1)}_{mj}}{\partial x_l} \right) \\
&= A_{im}\, \frac{\partial M^{(1)}_{mn}}{\partial x_l} \Big(M_{nj} + \delta_{nj} \Big) \, .
\end{aligned}
\tag{A.8}
$$

References

1. Bonnecaze, R. & Brady, J. A method for determining the effective conductivity of dispersions of particles. *Proceedings of the Royal Society of London. Series A: Mathematical and Physical Sciences* **430,** 285–313 (1990).

2. Bonnecaze, R. & Brady, J. The effective conductivity of random suspensions of spherical particles. *Proceedings of the Royal Society of London. Series A: Mathematical and Physical Sciences* **432,** 445–465 (1991).

3. Yurkovetsky, Y. & Brady, J. F. Statistical mechanics of bubbly liquids. *Physics of Fluids* **8,** 881–895 (1996).

A p p e n d i x B

RAYLEIGH DISSIPATION FUNCTION

The Rayleigh dissipation theorem [1, 2] allows us to include viscous dissipation in the Lagrangian framework. The viscous dissipation is derived via a balance of energy and is given by

$$\dot{\mathrm{E}}^{\mathrm{v}} = 2\,\mu \int \mathbf{e} : \mathbf{e}\; dV \;, \tag{B.1}$$

where superscript v denotes viscous effects and is not an index. The symmetric rate of strain tensor $\mathbf{e}$ double contraction can be rewritten in terms of the scalar potential as

$$\dot{\mathrm{E}} = 2\,\mu \int \nabla\nabla\phi : \nabla\nabla\phi \; dV \;. \tag{B.2}$$

The potential is once again expanded in a linear form of the boundary conditions (Eq. (2.8)), and the divergence theorem is applied to simplify Eq. (B.2) as

$$\dot{\mathrm{E}}^{\mathrm{v}} = -2\,\mu\, \boldsymbol{U}_\alpha \cdot \left(\int_{\partial\Omega_\lambda} (\nabla\nabla\boldsymbol{\Phi}_\alpha) : (\nabla\boldsymbol{\Phi}_\beta\, \boldsymbol{n}_\lambda)\, dS \right) \cdot \boldsymbol{U}_\beta \;. \tag{B.3}$$

The potential field is solved for the dipole disturbances via Faxén-type laws relating the potential at a particle center to the potential existing in at that same point in the absence of the particle [3]

$$\boldsymbol{\Phi}_\gamma\,(\boldsymbol{x}) = \frac{a^3}{2} \left(\nabla \frac{1}{|\boldsymbol{x} - \boldsymbol{R}_\nu|} \right) \cdot \left[\frac{2}{3}\, \boldsymbol{M}^{(1)}_{\nu\psi} \cdot (\boldsymbol{M}_{\psi\gamma} + \mathbf{I}\,\delta_{\psi\gamma}) + \mathbf{I}\,\delta_{\nu\gamma} \right] \;. \tag{B.4}$$

The dissipation rate is then written as a simple, quadratic form of the particle velocities

$$\dot{\mathrm{E}}^{\mathrm{v}} = \boldsymbol{U}_\alpha \cdot \boldsymbol{\mathcal{R}}_{\alpha\beta} \cdot \boldsymbol{U}_\beta \;, \tag{B.5}$$

where we group the integral and constants into the Rayleigh dissipation tensor $\boldsymbol{\mathcal{R}}_{\alpha\beta}$. Constant terms are removed from the integral and denoted via tensor $\boldsymbol{N}$ defined by

$$\boldsymbol{N}_{\nu\gamma} = \frac{2}{3}\, \boldsymbol{M}^{(1)}_{\nu\psi} \cdot (\boldsymbol{M}_{\psi\gamma} + \mathbf{I}\,\delta_{\psi\gamma}) + \mathbf{I}\,\delta_{\nu\gamma} \;. \tag{B.6}$$

Analytic solution of the Rayleigh dissipation tensor requires a Taylor expansion of the potential fields for a given particle pair ν and η located inside the integrand. The potential disturbances are both expanded about another

particle λ center whose surface is integrated over. In general, λ can be either ν, η, or both. The leading order expansions yield different analytical forms for each set of $\{\eta, \nu, \lambda\}$ particles depending on the their relationship and is summarized in tensor form as

$$\boldsymbol{C}_{\nu\eta;\lambda} = \begin{cases} -12\,\pi\,\mathbf{I} & \lambda = \eta,\ \nu = \eta \\ \mathbf{0} & \lambda = \eta,\ \nu \neq \eta \\ 8\,\pi\,\boldsymbol{M}^{(1)}_{\eta\nu} & \lambda = \nu,\ \nu \neq \eta \\ \frac{8\,\pi}{3}\,\nabla\boldsymbol{M}^{(1)}_{\lambda\nu} : \nabla\boldsymbol{M}^{(1)}_{\lambda\eta} & \lambda \neq \nu,\ \nu \neq \eta \quad (\lambda \text{ not summed over}) \end{cases} . \tag{B.7}$$

The semicolon denotes that the sub-tensor $\boldsymbol{C}_{\nu\eta}$ is parametrically dependent on the integration surface of particle λ. In the full Rayleigh dissipation tensor, all λ are summed over for each $\boldsymbol{C}_{\nu\eta}$ sub-tensor

$$\boldsymbol{\mathcal{R}}_{\alpha\beta} = a\,\mu \sum_{\lambda=1}^{N} \left(\boldsymbol{N}_{\alpha\nu} \cdot \boldsymbol{C}_{\nu\mu;\lambda} \cdot \boldsymbol{N}_{\mu\beta}\right) . \tag{B.8}$$

By the Rayleigh dissipation theorem, the viscous dissipative force can then be calculated via the velocity derivative as

$$\mathbf{F}^{\mathrm{v}} = -\frac{1}{2}\frac{\partial \dot{\mathrm{E}}^{\mathrm{v}}}{\partial \boldsymbol{U}} = -\boldsymbol{\mathcal{R}} \cdot \boldsymbol{U} . \tag{B.9}$$

Note that we recover the well-known isolated sphere viscous drag of $\mathbf{F}^{\mathrm{v}} = -12\,\pi\,a\,\mu\,\boldsymbol{U}$ (cf. Eqs. (B.6)–(B.8)).

References

1. Goldstein, H., Poole, C. & Safko, J. *Classical mechanics* (American Association of Physics Teachers, 2002).
2. Minguzzi, E. Rayleigh's dissipation function at work. *European Journal of Physics* **36,** 035014 (2015).
3. Yurkovetsky, Y. & Brady, J. F. Statistical mechanics of bubbly liquids. *Physics of Fluids* **8,** 881–895 (1996).

A p p e n d i x C

GENERALIZED WORK-ENERGY THEOREM

In Lagrangian mechanics, a generalized external force $\mathbf{F}$ can be added to a Lagrangian system as [1, 2]

$$\frac{d}{dt}\left(\frac{\partial \mathscr{L}}{\partial \dot{\boldsymbol{R}}}\right) - \frac{\partial \mathscr{L}}{\partial \boldsymbol{R}} = \mathbf{F} \ . \tag{C.1}$$

The work done by the generalized force is defined as the line integral of the force over a set distance from arbitrary state 1 to state 2

$$\mathrm{W} = \int_{x_1}^{x_2} \mathbf{F} \cdot d\boldsymbol{l} = \int_{t_1}^{t_2} \mathbf{F} \cdot \boldsymbol{U}\, dt \ . \tag{C.2}$$

In the special case where the particles posses no potential energy ($\mathscr{L} = \mathscr{T} = \frac{1}{2}\, U_j\, \mathscr{M}_{jk}\, U_k$) we evaluate the required derivatives in Eq. (C.1) with $\dot{\boldsymbol{R}} = \boldsymbol{U}$.

$$\begin{aligned} \frac{\partial \mathscr{T}}{\partial U_i} &= \frac{1}{2}\, \mathscr{M}_{ik}\, U_k + \frac{1}{2}\, U_j\, \mathscr{M}_{ij} = \mathscr{M}_{ij}\, U_j \qquad \text{by symmetry of } \mathscr{M} \\ \frac{\partial \mathscr{T}}{\partial R_i} &= \frac{1}{2}\, U_j\, \frac{\partial \mathscr{M}_{jk}}{\partial \mathrm{R}_i}\, U_k \end{aligned} \tag{C.3}$$

Substituting Eq. (C.1) into Eq. (C.2) and integrating for one period of a periodic oscillation yields

$$\begin{aligned} \mathrm{W} &= \int_{t_1}^{t_2} U_i\, \frac{d}{dt}\left(\mathscr{M}_{ij}\, U_j\right) dt - \int_{t_1}^{t_2} U_i \left(\frac{1}{2}\, U_j\, U_k\, \frac{\partial \mathscr{M}_{jk}}{\partial R_i}\right) dt \\ &= \int_{t_1}^{t_2} \frac{d}{dt}\left(U_i\, \mathscr{M}_{ij}\, U_j\right) dt - \int_{t_1}^{t_2} \left(\mathscr{M}_{ij}\, U_j\, \frac{dU_i}{dt} + \frac{1}{2}\, U_i\, U_j\, U_k\, \frac{\partial \mathscr{M}_{jk}}{\partial R_i}\right) dt \\ &= \left(U_i\, \mathscr{M}_{ij}\, U_j\right)\Big|_{t_1}^{t_2} - \int_{t_1}^{t_2} \left(\mathscr{M}_{ij}\, U_j\, \frac{dU_i}{dt} + \frac{1}{2}\, U_i\, U_j\, U_k\, \frac{\partial \mathscr{M}_{jk}}{\partial R_i}\right) dt \ . \end{aligned} \tag{C.4}$$

The remaining integral can be simplified using the product rule of derivatives as

$$\mathscr{M}_{ij}\, U_j\, \frac{dU_i}{dt} = \frac{d}{dt}\left(\frac{1}{2}\, \mathscr{M}_{ij}\, U_i\, U_j\right) - \frac{1}{2}\, U_i\, U_j\, U_k\, \frac{\partial \mathscr{M}_{jk}}{\partial R_i} \ . \tag{C.5}$$

The work over a given time-interval is then

$$\mathrm{W} = \frac{1}{2}\, \mathscr{M}_{ij}\, U_i\, U_j\Big|_{t_1}^{t_2} = \mathscr{T}\left(t_2\right) - \mathscr{T}\left(t_1\right) \ , \tag{C.6}$$

which is a generalization of the well known work-energy theorem in the case where the mass is a function of configuration. The work done on the particles by the generalized force is a state function of the kinetic energy evaluated at both ends of the interval of interest.

References

1. Minguzzi, E. Rayleigh's dissipation function at work. *European Journal of Physics* **36,** 035014 (2015).
2. Goldstein, H., Poole, C. & Safko, J. *Classical mechanics* (American Association of Physics Teachers, 2002).

A p p e n d i x D

OVERVIEW OF STOKESIAN DYNAMICS

The Stokes regime is defined as Re $\ll 1$ and inertial forces are negligible. The solution of the fluid velocity field reduces to Laplace's equation for the fluid flow field. As the Stokes regime is linear in the particle velocity vector (no-slip boundary conditions), we can decompose the motion of a solid body into a set of simpler motions, such as rigid translation and rotation [1, 2]. The longest-ranged fluid disturbance is due to translation and scales as a monopole, $O(r^{-1})$, at leading order, which is a much longer-ranged interaction than in a potential flow.

The velocity field is Taylor expanded in terms of particle surface velocity moments: linear velocity $\boldsymbol{U}$, rotational velocity $\boldsymbol{\Omega}$, symmetric rate of strain tensor $\mathbf{E}$, and higher order moments [3–5]. The force on the particle surface is similarly expanded in surface moments. In the numerical results presented, we follow the convention of only expanding to the first symmetric moment. This yields the commonly used F-T-S model (force, torque, and stresslet). The force moments can be related to velocity moments through linear relations (Faxén laws), and are summarized in grand tensional form by

$$\begin{pmatrix} \boldsymbol{U} \\ \boldsymbol{\Omega} \\ \mathbf{E} \end{pmatrix} = - \begin{pmatrix} \hat{\mathbf{M}}_{UF} & \hat{\mathbf{M}}_{UL} & \hat{\mathbf{M}}_{US} \\ \hat{\mathbf{M}}_{\Omega F} & \hat{\mathbf{M}}_{\Omega L} & \hat{\mathbf{M}}_{\Omega S} \\ \hat{\mathbf{M}}_{EF} & \hat{\mathbf{M}}_{EL} & \hat{\mathbf{M}}_{ES} \end{pmatrix} \cdot \begin{pmatrix} \mathbf{F} \\ \mathbf{L} \\ \mathbf{S} \end{pmatrix} , \tag{D.1}$$

with the so-called mobility tensor elements $\hat{\mathbf{M}}$ denoted with hats to avoid confusion with the added mass tensor in the potential fluid regime. It is important to note that the mobility tensor is only a function of particle configuration, just as the added mass tensor is in the potential regime. The mobility tensor physically captures the coupling between force and velocity and is derived in Ref. [5]. Without inertial forces, Newton's second law for the particles reduces to

$$\mathbf{F}^{\mathrm{H}} + \mathbf{F}^{\mathrm{P}} = \mathbf{0} , \tag{D.2}$$

where $\mathbf{F}^{\mathrm{H}}$ is the hydrodynamic force ($\mathbf{F}$ in Eq. (D.1)), and $\mathbf{F}^{\mathrm{P}}$ is any non-hydrodynamic force. Solution for the hydrodynamic force requires inversion of the mobility tensor to yield the resistance tensor $\hat{\mathbf{R}}$. The inversion captures the reflection of all interactions between solid particles, and allows one to solve for the particle velocities given a known $\mathbf{F}^{\mathrm{P}}$ via Eq. (D.2)

$$\boldsymbol{U} = \hat{\mathbf{R}}_{FU}^{-1} \cdot \left(\mathbf{F}^{\mathrm{P}} - \hat{\mathbf{R}}_{F\Omega} \cdot \boldsymbol{\Omega} - \hat{\mathbf{R}}_{FE} : \mathbf{E} \right) . \tag{D.3}$$

In many-particle systems, the resistance matrices are calculated numerically, and Eq. (D.3) provides an equation of motion in the Stokes regime.

References

1. Deen, W. M. *Analysis of transport phenomena* (Oxford University Press New York, 1998).
2. Happel, J. & Brenner, H. *Low Reynolds number hydrodynamics: with special applications to particulate media* (Springer Science & Business Media, 2012).
3. Swan, J. W., Brady, J. F., Moore, R. S. & 174, C. Modeling hydrodynamic self-propulsion with Stokesian Dynamics. Or teaching Stokesian Dynamics to swim. *Physics of Fluids* **23,** 071901 (2011).
4. Brady, J. F. & Bossis, G. Stokesian dynamics. *Annual review of fluid mechanics* **20,** 111–157 (1988).
5. Durlofsky, L., Brady, J. F. & Bossis, G. Dynamic simulation of hydrodynamically interacting particles. *Journal of fluid mechanics* **180,** 21–49 (1987).